Neurotoxicology 73 (2019) 213–227

Contents lists available at ScienceDirect

Neurotoxicology

journal homepage: www.elsevier.com/locate/neuro

Full Length Article

Zinc oxide nanoparticle induced neurotoxic potential upon interaction with primary astrocytes

S. Sudhakaran, S.S. Athira, P.V. Mohanan*

Toxicology Division, Biomedical Technology Wing, Sree Chitra Tirunal Institute for Medical Sciences and Technology, Poojapura, Trivandrum 695 012, Kerala, India

ARTICLE INFO

Keywords:
ZnO nanoparticles
Astrocytes
Neurotoxicity
Lysosomal stability
Caspase

ABSTRACT

As obvious from the basic prerequisite of any particle in nanoscale, Zinc oxide nanoparticles (ZnO NPs) possess numerous tunable properties distinct from their bulk formulations. Emerging innovations in various sectors of nanotechnology are exploiting ZnO NPs largely. This inturn picks up the occasions of human exposure irrespective of the application fields. Although the platform of nanotoxicology has been garnished with nano-bio interaction studies using different cell lines, a few are existing so far comprising primary cells which symbolize realistic *in vivo* environment. The present study addresses the neurotoxic potential of ZnO NPs using primary astrocytes isolated from post-natal 0–2 day old rat pups. Cells were cultured and maintained in DMEM F12 followed by purification. ZnO NPs generated by wet chemical method was then characterized both physico chemically and biologically. All of the techniques confirmed homogenous distribution of NPs and ensured enough colloidal stability. Bio-nano interaction studies commence on cell viability assays (MTT and NRU) and both of which confirmed dose and time dependent cytotoxicity. Alterations within cellular morphology, cytoskeletal arrangement, lysosomal stability, mitochondrial membrane potential (MMP) and caspase activation were evaluated by standardized techniques. All of the assays substantiated significant toxic consequences in astrocytes with characteristic hall marks. Apoptotic cell death was noted without any deformations of nuclear material. A comparative toxicity study using ZnO NPs, $ZnCl_2$ and ZnO bulk form was performed which confirmed nanospecific toxicity of ZnO NPs. Overall study evidently provide cautious information that ZnO NPs is capable of eliciting serious neuronal tissue damages which can turn out to be fatal during prolonged exposure.

1. Introduction

With the emergence of Scanning Probe Microscopy (SPM) in 1980s, the door towards nanoworld has widely opened. This later caused great revolutionary impacts in varied scientific as well as industrial disciplines. NPs which build the basement for nanoscience constitutes ultrafine particles fall in the nanoscale range of 1–100 nm. By the end of 20th century, Nanotechnology turned out to be one of the hot topics among scientific community and led to the development of an array of great inventions (Bao et al., 2013). Along with the advent of Nanotechnology, newer and pioneer NPs got formulated and flourished different application fields. Unique structural and functional properties of NPs like high surface area/volume ratio, tunable shapes and surface characteristics, electronic and thermal conductivity, quantum confinement effect *etc*., make them ideal nominee for wide variety of applications (Schummer, 2004). Broad variety of NPs have already thrived our day-to-day life such as in electronic devices, optical devices, sensors, clothes, sunscreens, food products as well as medicines. According to Consumer Product Inventory (CPI) report in 2015, roughly about 1600 types of Nanotechnology based products are available in market nowadays (Vance et al., 2015).

Based on the composition and performances, NPs could be largely categorized as organic and inorganic. Among the mostly studied inorganic NPs, metals and their oxides, semiconductor NPs and some minerals and silica should be mentioned foremost (Buzea et al., 2007). One of the common possessions exhibited by NPs is their higher surface energy due to the peculiar electron distribution pattern. This in turn leads them thermodynamically unstable and highly surface reactive (Nohynek et al., 2008).

Nanotoxicology has emerged as a mandatory requirement after commercialization of many nanotechnology derived products. The severity of toxicological consequences of NPs during interaction with biological systems could be considered as the function of the physicochemical properties of them. Thus NPs interact with biological system in unpredictable ways with varied severity extremes. For instance, Gold is an inert material whereas its nano form is considered as highly

* Corresponding author.
E-mail address: mohanpv@sctimst.ac.in (P.V. Mohanan).

https://doi.org/10.1016/j.neuro.2019.04.008
Received 24 January 2019; Received in revised form 11 April 2019; Accepted 23 April 2019
Available online 25 April 2019
0161-813X/

reactive (Panyala et al., 2009). NP mediated toxicity occurs primarily *via* reactive oxygen species (ROS) generation and subsequent complications including mitochondrial and membrane damage, lysosomal destabilization, inflammatory responses and genotoxicity (Manke et al., 2013). Risk factors of NPs comprise their ability to breach biological barriers like Blood Brain Barrier (BBB) and placenta. It has been reported that NPs localize in brain to induce oxidative stress and protein fibrillation which all could be linked to neurological pathologies (Soenen et al., 2011).

ZnO NP; one of the wide band gap semi conductor materials (energy gap 3.37 eV at room temperature) have caught noteworthy attention owing to its magical functional and structural properties. ZnONPs have been used as active mediator for applications like UV absorption, catalysis, sensor manufacturing and in photo electronic devices from decades back (Wang, 2004). Moreover they are being applied in several biological disciplines like drug delivery, phototherapy as well as in biosensing. ZnO NPs are proposed to be an effective cancer therapeutic agent. They exhibit preferential toxicity on cancer cells compared to normal cells (Hanley et al., 2008). These particles are well known for their anti-bacterial property owing to the capabilities of photocatalysis and reactive oxygen species (ROS) generation. High positive charge of the particle surface underlies their ability to interact with negative surface of both bacterial cell wall and cancer cells. This consecutively leads to bactericidal activity and cancer destruction respectively (Sirelkhatim et al., 2015). Antibacterial agents containing ZnO NPs are used in dental composites and daily care products such as mouthwash, diapers and shampoos (Hernández-Sierra et al., 2008). Humans thus become exceedingly liable to ZnO NP exposure predominantly because of such inevitable usages.

Considering the toxicological profile of ZnO NPs, they have reported to be causing ROS mediated single stranded DNA breaks even at a relatively lower concentration of 10 μg/ml (Chang et al., 2012). Recent researches show that NPs enter into brain loci *via* systemic circulation and olfactory neuronal pathways. Particularly ZnO NPs have proven to induce cytotoxicity in neuronal progenitor cells and neurons (Deng et al., 2009). In human neuroblastoma SHSY5Y cells, ZnO NPs induced oxidative stress, genotoxicity, cell cycle alteration and apoptosis in a time and dose dependent manner. However the study failed to address the particle internalization by the cells (Valdiglesias et al., 2013). In mice model with depressive-like behaviour, the ZnO NPs reached brain after oral and inhalation exposure, where it interfered an altered spatial learning and memory by altering synaptic plasticity (Xie et al., 2012). Major share of existing data came from *in vitro* studies which concentrate more on neuronal cell lines. Studies on primary brain cell cultures mimicking the exact neuronal tissue environment are still lagging behind. During most of the circumstances this could be because of the complexity in maintaining primary cultures along with their extreme nutritional requirements (Fröhlich, 2018). However inorder to obtain relatively more reliable results, it is always apparent to use primary cell cultures for cytotoxicity studies rather than immortalized or transformed cell lines. Considering the neuronal tissue in particular, astrocytes constitute the abundant glial cells. They perform a verity of functions in CNS ranging from axon guidance and synaptic support to BBB integrity maintenance and metal homeostasis (Blackburn et al., 2009). Astrocytes facilitate long term recovery during brain injury by surface molecule expression and release of trophic factor. Due of these functional properties it is essential to assess their toxic vulnerability due to potent agents.

The present study introduces the neurotoxic potential of ZnO NPs upon interaction with primary astrocytes isolated from post-natal 0–2 day old rat pups. Major cytotoxicity assays include assessment of cell viability, free radical generation, cytoskeletal arrangement, subcellular integrity, nuclear stability, caspase activity and apoptosis. Impact of NP size and colloidal stability on cytotoxicity as well as comparative cytotoxicity investigation using ZnO NPs, $ZnCl_2$ and ZnO bulk formulation is also need to be addressed.

2. Materials and methods

2.1. Materials

Sodium hydroxide, zinc chloride, zinc sulphate, zinc nitrate, sodium nitrate, RPMI-1640 media, (3-(4,5-Dimethylthiazol-2-yl)-2,5-Diphenyltetrazolium Bromide)/ MTT, Griess reagent, Histopaque, sodium dodecyl sulphate (SDS), thiobarbituric acid, acrylamide, bis acrylamide, TEMED (Tetramethylethylenediamine), tris base, trypan blue, Evan's blue were purchased from Sigma (USA). Endosafe PTS kit was acquired from Charles River (USA). Dil-Ac-LDL and Cytopainter phalloidin were obtained from Abcam (UK). Dulbecco's Modified Eagle's Medium F12 (DMEM F12), fetal bovine serum (FBS), antibiotic/antimycotic, glutamax, phosphate buffered saline, 0.25% trypsin were obtained from gibco®, Life technologies (USA), calcien AM, JC-1 Dye (Mitochondrial Membrane Potential Probe)and apoptotic DNA ladder kit was purchased from ThermoFisher Scientific (USA). Coomassie brilliant blue and Folin's reagent were bought from Merck, India. Haematoxylin, eosin neutral red, propidium iodide, ethidium bromide and DAPI (4′,6-diamidino-2-phenylindole) were purchased from Himedia, India. SensoLyte ® Homogeneous AMC Caspase-3/7 Assay Kit was procured from AnaSpec, USA.

2.2. ZnO NP synthesis and characterization

2.2.1. ZnO NP synthesis

Wet chemical method (Narkiewicz et al., 2008) was adopted for ZnO NP generation using zinc sulphite ($ZnSO_4$) as zinc salt and NaOH as reducing agent. For that, 100 ml each of 0.05 M (718.8 mg) $ZnSO_4$ and 0.15 M (300 mg) NaOH (1:3 M ratio) solution was prepared in deionised water. The $ZnSO_4$ solution was heated to 90 °C. While maintaining the temperature, NaOH solution was added to the $ZnSO_4$ solution in a single step. The reaction mixture was kept under constant stirring for 2 h at 860 rpm (95x g). The solution was allowed to cool down and pH was monitored. ZnO NPs synthesized by this method was centrifuged at 10,000 rpm (12857x g) for 10 min to remove unreacted precursors. Dialysis (membrane pore size: 3.5 kD) was carried out using the white precipitate for 1 week followed by ultra filtration (6 times). Conductivity of the ultra-filtrate was recorded and the concentration of ZnO NPs in solution was determined by taking dry weight.

2.2.2. Physico-chemical characterization

The sysnthesized ZnO NPs were characterized for their physico-chemical properties like size, morphology, structure, surface charge, colloidal stability, surface area and purity using varying techniques. Surface morphology of ZnO NPs was evaluated using SEM, JEOL JSM-6400 F (JEOL, USA) operating at accelerating voltage in the range of 0.5–30 kV. Size of the particle was determined by Transmission electron microscopy (TEM); JEOL JEM-2100 LaB6 (JEOL, USA. Average size of the particles was calculated using Image J software. Hydrodynamic diameter of the nanoparticle in water, PBS and cell culture medium was measured by Zetasizer Nano ZS (Malvern, USA) supplied by DTSNano V4.2 software. Also DLS measurements were done by dispersing different concentration of ZnO NPs in water to study the effect of concentration and particle aggregation on hydrodynamic diameter. The dispersity of particle in solution was analysed from the Poly Dispersity Index (PDI). Zeta potential (ζ) was measured over different pH using a Zetasizer Nano ZS (Malvern, USA) instrument supplied by DTS Nano V4.2 software. XPS (X-ray photo electron spectroscopy) analysis of ZnO NPs was done by PHI Verasaprobe 5000 (ULVAC-PHI, INC, Japan) with aluminium Al κα1.

2.2.3. Biological characterization

2.2.3.1. Endotoxin detection. The toxicity analysis of NPs is typically found to be influenced by the endotoxins contained in them. For the present study, endotoxin content of ZnO NPs was assessed using Charles

River Endosafe PTS kit. Endotoxin present in the sample reacts with the Limulus ameobocyte lysate and form a gel clot. The gel clot formed corresponds to the endotoxin contained in the sample. ZnO NPs (100 µg/ml) were dispersed in endotoxin free water. These particles were centrifuged at 14,000 rpm (17999x *g*) for 15 min. Endotoxin contamination was analysed using the supernatant. 25 µl of the supernatant was added to the cartridge well and loaded on to the Endosafe PTS. Readings were taken and the endotoxin content was expressed in EU/ml.

2.3. Isolation of astrocytes

Primary astrocytes were isolated from post-natal 0–2 day old rat pups according to protocol described by Weinstein DE (Weinstein, 2001) with slight modifications. The pups were decapitated using scalpel blades. The head was transferred to 70% alcohol. In sterile hood, downstream isolation procedures were carried out by placing on ice. Whole brain was isolated intact and the meningeal layer was carefully stripped off in cold HBSS (Hanks Balanced Salt Solution) with the aid of forceps. The tissues were subjected to mechanical mincing using a scalpel blade and followed by enzymatic digestion using 0.25% trypsin at 37 °C for 10 min. 0.02% deoxyribonuclease was added to the solution and cell suspension was triturated using fire polished pasture pipettes. The single cell suspension was transferred to a fresh tube by passing through a 70 µm nylon mesh. The cells were centrifuged at 1700 rpm (333x g) for 5 min and resuspended in complete medium containing DMEM F12 supplemented with 10% heat-inactivated FBS (fetal bovine serum), 1% penicillin/streptomycin and 1% glutamax. The cell suspension was pelleted and re-suspended in fresh complete medium. The suspension was filtered through a 100-µm nylon membrane and plated into T75 culture flasks. The culture was kept undisturbed for 7 days in a 5% CO_2 incubator at 37 °C.

2.4. Primary astrocytes purification

Loosely adherent microglia and oligodendrocyte were eliminated by chemical and mechanical means. The cells on attaining complete confluency were treated with 50µM L-leucine methyl ester (LME) for 1 h. The LME is a lysosomotropic agent which selectively kills microglia. After treatment, the medium was discarded and the flask was rinsed using HBSS. The cells were harvested by trypsinisation and sub-cultured at 1:2 dilutions. The first passage on reaching confluency were covered using a cling film to stop gaseous exchange with environmental air and kept on an incubator shaker at 37 °C and 260 rpm (9x g) for 24 h. This shaking process dislodges the loosely adherent microglia and oligodendrocytes in the culture (Foo et al., 2011). After discarding the medium, the cells were washed using sterile HBSS and sub-cultured at 1:2 dilutions.

2.5. Characterization of primary astrocytes

Astrocyte specific marker Glial Fibrillary Acid Protein (GFAP) was used to characterize primary astrocytes and β-tubulin was employed to identify the neurons. Cells were seeded at a density of 1×10^5 cells/well on cover slip and incubated overnight. Before removing the complete medium, cells were incubated with 4% formaldehyde (in water) for 4 min to minimize the cell damage during fixation. Medium was discarded and cells were washed with sterile HBSS (3 times in 3 min gap). Cells were later fixed using 1.2% formaldehyde for 15 min. The excess aldehyde was quenched by adding 0.1 M glycine (in PBS) for 5 min. Cells were treated with BP (Blocking and Permeabilisation) solution for 30 min at room temperature to permeabilize the cells and block the unwanted sites. The BP solution was prepared by adding 200 µl of Triton X 100 and 500 µl of 5% FBS and was made up to 10 ml in 1X PBS. After removing the BP solution, primary antibody (1:500 dilutions in PBS) was added to the wells and incubated overnight (not less than 16 h) at 4 °C. The cells were washed thrice with PBS (in 3 min gap) and incubated with secondary antibody (1:500 dilutions in PBS) in dark for 2 h at room temperature. Nucleus of the cells was demarcated using 1 µl of DAPI (1 mg/ml) for 5 min. The cells were washed thrice with 1X PBS and observed under microscope using blue and green filter.

To analyse the proportion of neuronal population, cells were seeded separately and stained for the neuronal marker β3 tubulin following the same procedure described above. Cell surface marker O4 antibodies were used as oligodendrocyte marker. The staining procedure was same as that described above except for the permeabilisation step. The antibody was diluted in PBS containing 5% FBS. The acetylated low density lipoproteins conjugated with fluorescent probe 'Dil' (Dil-Ac-LDL) were used to identify contaminating microglia and endothelial cells. These cells internalize the Dil-Ac-LDL by scavenger receptor and metabolize the Dil-Ac-LDL resulting in intracellular accumulation of 'Dil'. The cells were incubated with 10 µg/ml of Dil-Ac-LDL for 4 h at 37 °C and 5% CO_2. 1 µg/ml of DAPI for 5 min was used to demarcate the nucleus in all experiment. The cells were washed using PBS and observed under microscope (Axio Scope.A1, Carl Zeiss, Germany).

2.6. Cell culture and ZnO NP treatment

Cells were maintained in T25 flask containing complete medium (DMEM F12 with 10% heat-inactivated FBS (fetal bovine serum), 1% penicillin/streptomycin and 1% glutamax). The culture from 4th to 8th passage with 70–80% confluency was used for further *in vitro* experiments. Cells having an initial density of 1×10^4 cells/well and 5×10^5 cells/well were seeded into 96 well and 4 well plates respectively. Whereas for 6 well plates, 1×10^5 cells/well were seeded. After overnight incubation, cells were exposed with varying concentrations of ZnO NPs like 1, 5, 10, 20, 40 and 80 µg/ml.

2.7. Cell viability and dose response

2.7.1. MTT assay

Cell viability was assessed as a function of percentage mitochondrial activity using MTT (3-(4, 5-Dimethylthiazol-2-yl)-2, 5-Diphenyltetrazolium Bromide) assay. The assay principally relies on colorimetric measurement of purple colored (E, Z)-5-(4, 5-dimethylthiazol-2-yl)-1, 3-diphenyl formazan crystals formed *via* the reduction of yellow tetrazolium dye MTT by NAD (P) H-dependent cellular oxido-reductase enzyme present in metabolically active cells (Bahuguna et al., 2017). In brief, cells were seeded at an initial density of 1×10^4 cells/well and incubated overnight at 37 °C atmosphere bounded with 5% CO_2. Cells were then exposed to varying concentrations of ZnO NPs (1, 5, 10, 20, 40 and 80 µg/ml) and incubated for different time periods like 3, 6 and 24 h in order to compare the time responsive impact of the NPs on primary astrocytes. In addition, particle interference on MTT reagent has nullified by parallely treating the NPs alone of each concentration prepared in DMEM; which served as the NP blank. The medium was replaced with 100 µl MTT (50 µg/ml in medium) and incubated for 3 h in dark. Medium was discarded and the formazan crystals formed were solubilized using DMSO (100 µl/well, incubated in dark for 15 min). The Spectrophotometric measurement was taken at 540 nm using ELx 808 ultra-microplate reader (Biotech instruments, USA).

2.7.2. Neutral red uptake (NRU) assay

Lysosomal activity of the metabolically active cells was evaluated by the method adopted from Borenfreund and Puerner (Borenfreund and Puerner (1985)). Cells cultured at an initial density of 1×10^4 cells/well were incubated with 5, 10, 20, 40 and 80 µg/ml ZnO NPs for 3, 6 and 24 h at 37 °C. NP blank was also employed as mentioned in section **2.7.1.** 10 µl of 1% neutral red was added to each well and incubated in dark for 3 h. Consequently, the cells were washed with PBS and the dye taken up by the cells were solubilized using 100 µl acid alcohol (1%, v/

v, acetic acid and 50% ethanol) by keeping the cells on an incubator shaker at 60 rpm (2x g), 37 °C for 30 min. Absorbance was measured at 540 nm using a ELx 808 multiwell plate reader (Bio-Tek, Winooski, USA).

2.8. Particle uptake in presence of inhibitor

In order to analyze the endocytic pathways of ZnO NPs, Cytochalasin D (Cyt. D); which is a well-known cell permeable mycotoxin that inhibits actin polymerization was exposed to cells. It is a non-specific inhibitor of endocytic pathway. Cells were seeded at an initial density of 1×10^4 cells/well and allowed to incubate overnight. Pre-incubation of cells was performed using 5 μM Cyt. D for 4 h. Cells were subsequently exposed with different concentrations of ZnO NPs (5, 10, 20, 40 and 80 μg/ml) for 24 h and NRU assay was carried out as mentioned in Section 2.7.2.

2.9. Cell morphology analysis by Giemsa staining

Cells having an initial density of 1×10^5 cells/ well were seeded onto coverslips placed on 6-well plate and placed overnight for attachment. Different concentrations of ZnO NPs (5, 10, 20, 40 and 80 μg/ml) were exposed to cells and incubated for 6 and 24 h. Cells were fixed using 4% formaldehyde for 15 min followed by PBS washing. Fixed cells were then stained with 10% Giemsa for 5 min and washed. After washing the slides thrice in PBS, morphology of cells were analyzed using compound microscope (Olympus CX31, Japan).

2.10. Cytoskeletal analysis by Rhodamine Phalloidin staining

Rhodamine phalloidin staining was performed to analyze the impact of ZnO NPs on cytoskeletal integrity of astrocytes. Phalloidin is a peptide toxin isolated from *Amanita phalloides.* This toxin is conjugated with the fluorescent moiety rhodamine to visualize the actin filaments by fluorescent microscopy (Reshma et al., 2016). Cells seeded at an initial density of 1×10^5 cells/well were exposed with ZnO NPs prepared in different concentrations (5, 10, 20, 40 and 80 μg/ml) and incubated for 6 and 24 h at 37 °C/5% CO_2 atmosphere. After PBS washing, cells were fixed using 3.7% formaldehyde for 10 min. In order to quench excess aldehyde, 0.1 M glycine (in PBS) was used for 5 min. Cells were permeabilised using 0.1% Triton-X 100 (in PBS) for 1 min. Cells were then stained with Rhodamine phalloidin (1:250 in PBS) for 15 min. After PBS washing, morphological analysis was performed using fluorescent microscope under red filter (Axio Scope.A1, Carl Zeiss, Germany).

2.11. Detection of reactive oxygen species (ROS) using DCFH-DA

ZnO NP induced ROS generation was evaluated using DCFH-DA by flow cytometry following the method of Wan et al. (Wan et al., 1993). In brief, 1×10^5 cells were incubated with varying concentrations of ZnO NPs (5, 10, 20, 40 and 80 μg/ml) for 6 h. After trypsinization, cells were washed with PBS and incubated with 1 μM DCFH-DA for 45 min at 37 °C. Washed and resuspended the cells in 200 μl cold PBS and measured immediately using BD FACSAria™, (BD BioSciences, USA) at an excitation and emission wavelength of 495 nm and 529 nm respectively. Gating was done with respect to positive control (freshly prepared 0.1 mM H_2O_2).

2.12. Detection of reactive nitrogen species (RNS) by Griess reagent assay

Nitric oxide species generation upon ZnO NP exposure was evaluated using Griess reagent method (Bryan and Grisham, 2007). Cells at an initial density of 1×10^4 cells/ well were seeded into a 96 well plate and incubated overnight. ZnO NPs prepared in different concentrations (5, 10, 20, 40 and 80 μg/ml) were exposed to cells and incubated for 6 h and 24 h. 50 μl each of cell supernatant and Griess reagent (1:1 ratio) were mixed and incubated at room temperature for 10 min. Absorbance was read at 540 nm using a multi well plate reader (Bio-Tek, Winooski, USA). The concentration was calculated from the sodium nitrate (0.5, 2.5, 5 and 7.5 μg/ml) standard graph. LPS (1 μg/ml) treated samples were used as positive control.

2.13. Assessment of lysosomal integrity using Acridine orange (AO) staining

Integrity of lysosomes was evaluated using a metachromatic dye AO which specifically binds with lysosome due to proton trapping. This caused the change in fluorescence from cytosolic green to red within the lysosomes (Sohaebuddin et al., 2010). Cells having an initial density of 5×10^4 cells/well were seeded into 4 well plates and allowed to incubate overnight. Different concentrations of ZnO NPs were prepared (5, 10, 20, 40 and 80 μg/ml) and exposed to the incubated cells for 6 h. After incubation, cells were incubated with AO (2 μg/ml in citrate phosphate buffer) for 15 min at 37 °C. Cells were washed with PBS and observed under fluorescent microscope under green and red filters (Axio Scope.A1, Carl Zeiss, Germany).

2.14. Mitochondrial membrane potential (MMP) evaluation by JC-1 staining

The cyanine dye JC-1 (5,5′,6,′-tetrachloro-1,1′,3,3′-tetraethylbenzimidazolyl-carbocyanine iodide) is well known for its ability to discriminate between energized and de-energized mitochondria. The dye exists in its polymerized form in the presence of energized mitochondria and exhibits red color. Whenever the mitochondria get de-energized, the dye shows a slight shift from red to green due to conversion of its polymeric to monomeric forms (Perelman et al., 2012). In short, Astrocytes were seeded at an initial density of 1×10^4 cells/well and exposed to ZnO NPs (5, 10, 20, 40 and 80 μg/ml) for 6 h and 24 h. At the end of exposure, 1 mM JC-1 dye was added to each well and incubated for 20 min at room temperature. After PBS washing, cells were observed under fluorescent microscope (Axio Scope.A1, Carl Zeiss, Germany) using green and red filters.

2.15. Apoptosis by annexin V/PI staining

Apoptosis in primary astrocytes exposed to ZnO NPs was analyzed using flow cytometry, BD FACSAria™ (BD BioSciences, USA). Phosphatidyl serine (PS) is a residue normally found on the inner surface of plasma membrane. During apoptosis, PS will get exposed to outer cellular environment. Annexin V is a cell-impermeant 35–36 kDa protein that possesses strong affinity towards PS. PI on the other hand is permeable to cells having a ruptured membrane (Biosciences, 2011). The present assay was carried out as per the manufacturer's instructions with slight modification. Astrocytes were seeded at an initial density of 1×10^4 cells/well and incubated for 24 h. During the end of incubation, cells were harvested by trypsinisation and centrifuged at 1700 rpm (333x g) and washed with cold PBS. After removing the medium, cells were stained with 5 μl of Annexin V for 10 min. 1 μl of PBS (100 μg/ml) constituted in 1X Annexin binding buffer (ABB) was added to each tube and incubated for 5 min. Treated cells were then kept in ice and instantly analyzed using FACS at an emission wavelength of 530 and 575 nm for Annexin V and PI respectively. Four controls were used for gating: cells alone, cells with Annexin V, cells with PI and cells with both Annexin V and PI. Subsequent to FACS analysis, microscopic observation was performed to confirm Annexin V/ PI staining.

2.16. Caspase 3/7 activation assay

Caspase 3 and 7 are two assassins act specifically on the downstream of caspase dependent apoptosis signaling cascade. Caspase 3/7 pathway activation during ZnO NP exposure on astrocytes was assessed

by the Ana spec SensoLyte® Homogeneous AMC caspase 3/7 assay kit as per manufacturer's instructions. Varying concentrations of ZnO NPs (5, 10, 20, 40 and 80 μg/ml) were exposed to Astrocytes in 96 well plates and incubated for 60 min in a plate shaker. Reading was obtained using a fluorescent plate reader (Tecan Infinite M200, Switzerland) at an excitation/emission wavelengths of 354/442 nm respectively. Caspase activity was evaluated by normalizing against total protein.

2.17. Cell membrane integrity by calcein AM-PI staining

NP induced membrane damage was assessed by double staining with calcein AM and PI (Propidium Iodide). Calcein AM is a widely accepted indicator of cell viability owing to its excellent retention capabilities and relatively high insensitivity to slighter fluctuations in physiological pH. This probe is also ideal for analysing cell adhesion, chemotaxis and multi drug resistance. Calcein upon hydrolysis by cellular enzyme is converted into a polyanionic fluorescein derivative that has about six negative charges and two positive charges at pH 7. PI (propidium iodide) on the other hand, penetrates the cells with compromised membrane integrity (De Simone et al., 2013). 20, 40 and 80 μg/ml of ZnO NPs were exposed to cells seeded at a density of 1×10^5 cells/well for 6 and 24 h. After emptying the culture plate, cells were washed with PBS. Cells were incubated with Calcein AM for 40 min at 37 °C followed by treatment with PI for 5 min. After PBS wash, cells were mounted for fluorescent microscopy (Axio Scope.A1, Carl Zeiss, Germany) using green and red filters.

2.18. Evaluation of nuclear condensation by DAPI staining

Chromosome condensation is a conventionally used marker for the primary evaluation of apoptosis. DAPI (4, 6-Diamido-2-phenylindole dihydrochloride) is one of the best nuclear binding dyes used for the fluorimetric detection of nuclear material condensation (Toné et al., 2007). Astrocytes seeded at an initial density of 1×10^5 cells/well were incubated with 20, 40 and 80 μg/ml ZnO NPs for 6 and 24 h. The medium was discarded and cells were washed with PBS. The cells were fixed using 4% formaldehyde and stained with DAPI (1 μg/ml) for 5 min. After washing with PBS, cells were observed under fluorescent microscope, Axio Scope.A1 (Carl Zeiss, Germany) using blue filter.

2.19. Effect of particle size and dissolution on astrocytes

Inorder to study the impact of particle size on cytotoxicity, ZnO NPs were compared with its bulk formulations (0.7–1.5 μM). Simultaneously, the effect of dissolution property of the particle on cytotoxicity was analysed by using $ZnCl_2$ which is a salt of zinc and readily dissociates in water to form zinc ion.

2.19.1. Cytotoxicity assessment by MTT assay

Different concentrations of ZnO NPs, ZnO bulk and $ZnCl_2$ (1, 5, 10, 20, 40 and 80 μg/ml) were exposed to astrocytes seeded at an initial density of 1×10^4 cells/well. Percentage of cell viability was evaluated by MTT assay after 6 and 24 h exposure as described in Section 2.7.1.

2.19.2. Determination of cell count by Trypan blue exclusion assay

Total cell count as a function of toxicity was carried out using trypan blue exclusion assay. Trypan blue is a vital dye which is impermeable to cells with intact membrane. Thus it enters into dead cells effortlessly and stains blue whereas live cells remains colorless.

The cells were seeded at an initial density of 1×10^6 cells/well were exposed to ZnO NPs, $ZnCl_2$ and ZnO bulk particles at 1, 5, 10, 20, 40 and 80 μg/ml for 24 h. The cells were harvested by trypsinisation and centrifuged at 1700 rpm (333x g) and pellet thus obtained was re-suspended in 200 μl PBS. Cell suspension was mixed with trypan blue in 1:1 ratio and cell count was obtained under phase contrast microscope (Axiovert 40 CFL, Zeiss) using Neubauer counting chamber.

2.19.3. Detection of ROS by DCFH-DA assay

ROS generated in presence of ZnO NPs, ZnO bulk and $ZnCl_2$ were detected using DCFHDA probe. Astrocytes seeded at an initial density of 1×10^4 cells/well were allowed to attach overnight and exposed to particles for 6 and 24 h. Measurement of ROS was performed as per Section 2.12.

2.19.4. Evaluation of proliferative capacity and survival rate by Clonogenic assay

The clonogenic assay was carried out to determine the effect of ZnO NPs, ZnO bulk and $ZnCl_2$ on growth and survival of the cells. Single cell suspensions of astrocytes were seeded in 6 well plates at a density of 2×10^4 cells/well. Astrocytes immediately after seeding were exposed to 10, 20, 40 and 80 μg/ml of ZnO NPs, ZnO bulk and $ZnCl_2$ for 3 h. The cells were subsequently replated at a density of 200 cells/well in 6 well plates. The dishes were left in incubator maintained at 37 °C with 5% CO_2 supply until the cells in control plates formed adequately large number of clones (clones containing more than 50 cells wereconsidered as representative of viable cells).

2.19.5. Evaluation of apoptosis by Caspase 3/7 activation assay

Caspase 3/7 activity in response to ZnO bulk formulation and zinc salt ($ZnCl_2$) was detected using SensoLyte Homogeneous AMC Caspase - 3/7 Assay Kit as section **2.17.** Cells were seeded at an initial density of 1×10^4 cells/well and incubated for 24 h. The results were compared with caspase activity on ZnO NPs exposure.

2.20. Statistical analysis

All the experiments were done in triplicates and values expressed as mean ± SD. Statistical comparison between the control and experimental values were done using students't-test. Analysis $p < 0.05$ was considered significant in results.

3. Results

3.1. Synthesis of ZnO NPs

ZnO NPs synthesized by wet chemical method was white in color and sparingly soluble in water. NPs showed a characteristic sphere head morphology (ZnO SP). The solution thus obtained was subjected to dialysis for 1 week followed by ultracentrifugation. The conductivity and pH of the ultra filtrate was 2.17 and 7 respectively which was comparable to that of ultra pure de-ionized water (Table 1). This further ensured the complete removal of unreacted residues from the sample.

3.2. Physico- chemical characterization

According to TEM analysis, ZnO SPs exhibited a narrow size distribution bearing an average size of 20 nm (Fig. 1a). Surface morphological evaluation of ZnO SPs was carried out by SEM. The NPs were found to be uniformly distributed and exhibited uniform morphology. Characteristic sphere head morphology was identified among the individual NPs (Fig. 1b). DLS data showing average hydrodynamic diameter and poly dispersity index (PDI) of ZnO SP in water, physiological saline and cell culture medium is given in Table 2.

The zeta potential of ZnO SP was measured over a range of pH, 2 to

Table 1
Comparison of conductivity and pH of ZnO NPs and ultra pure de-ionized water.

Sample	Conductivity (μS/m)	pH
ZnO SP	2.17	7
dH_2O	2.5	7

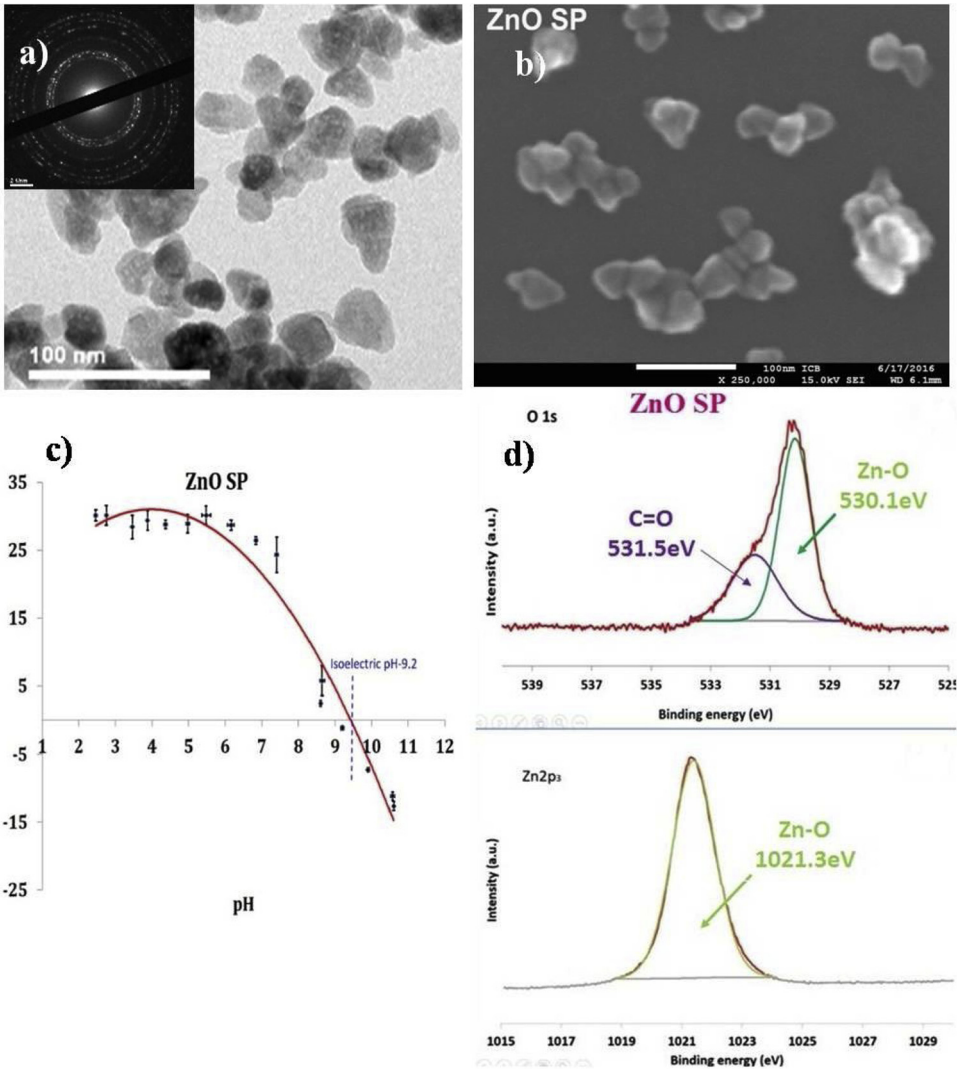

Fig. 1. (a) TEM image of ZnO NPs spherehead (ZnO SP); inset shows different patterns of ZnO SP. Magnification 50k. (b) Morphology of ZnO SPs using SEM analysis (c) Zeta potential of ZnO SPs (d) XPS analysis of ZnO SPs: i) O1s spectra of ZnO SPs ii) Zn_2P_3 spectra of ZnO SP.

Table 2
Effect of dispersant on hydrodynamic diameter and polydispersity index (PDI) of ZnO SP using DLS.

Sample	Parameters	Dispersant		
		Water	Saline	DMEM F12
ZnO SP	Z average dm (nm)	111.0 ± 2.06	603.0 ± 14.2	436.2 ± 3.11
	PDI	0.113 ± 0.01	0.347 ± 0.04	0.420 ± 0.02

11and it was found to be varied from 30 to -25 in 2 to 11. The particles showed a positive charge at physiological pH (Fig. 1c). The purity of ZnO SP was analysed by XPS. The binding energies were corrected using the adventitious peak at 284.8 eV of graphitic carbon. Peaks of oxygen n and zinc spectra were fitted using binding energies of different components present (Fig. 1d). O1s spectra of ZnO SP indicated two components with binding energies of 530.1 eV and 531.5 eV corresponding to oxides and surface adsorbed carbonates respectively. The binding energy of 1021.3 eV corresponding to Zn-O were shown in Zn_2P_3 spectra of ZnO SP.

3.3. Biological characterization

3.3.1. Endotoxin content

PTS method was used to determine the level of endotoxin present in the sample since it could have significant impacts in toxicity data of the particle. The results of the assay indicated that the endotoxin level was ≤ 0.05 EU/ml in both ZnO SP and $ZnCl_2$ which is well below the USP (United States Pharmacopeia) recommended level.

3.3.2. Effect of cell culture media on size of the nanoparticle

Composition of the cell culture media and incubation time influence the size and stability of the NP to a great extent. ZnO NPs were cultured in both DMEM F12 and RPMI 1640. Data showing the variation in size of NP according to the cell culture media and incubation time is illustrated in Table 3. It was observed that size of the NP fluctuated overtime in RPMI media whereas in DMEM, it remained more or less similar.

3.4. Isolation and purification of primary astrocytes

Astrocytes isolated from the whole brain of post-natal 0–2 day old rat pups were cultured in DMEM F12 medium supplemented with 10% FBS (Fig. 2a). The medium was replaced with fresh medium in every 3 days. The astrocytes exhibited a doubling time of 36 h. 70–90%

Table 3
Effect of cell culture medium on the size of nanoparticles: polydispersity index (PDI) of ZnO NPs by DLS.

Sample	Time of exposure	Z average (nm)	PDI
RPMI	5 min.	441.58 ± 3.44	0.51 ± 00
DMEM F12		380.25 ± 3.44	0.47 ± 00
RPMI	30 min.	633.72 ± 13.1	0.31 ± 0.05
DMEM F12		379.11 ± 5.72	0.45 ± 0.01
RPMI	60 min.	620.04 ± 7.44	0.29 ± 0.03
DMEM F12		378.35 ± 6.37	0.44 ± 0.02
RPMI	24 h	609.18 ± 2.26	0.28 ± 0.01
DMEM F12		372.25 ± 2.31	0.38 ± 0.04

confluent cells were used for characterization and bio assays.

3.5. Characterization of primary astrocytes

Immunocytochemistry method was adopted for the characterization of primary astrocytes. Different cell markers were used for the identification of purified astrocytes in the system. Presence of green colored GFAP marker confirmed the presence of astrocytes whereas cells remained negative for the neuronal marker β3 tubulin and oligodendrocyte marker O4 antibody indicating the absence of both these cell types in the culture (Fig. 2b). A few Ac-LDL positive cells (red) were present in the samples suggesting the presence of small fraction of microglia or endothelial cells.

3.6. Cell viability and dose response

3.6.1. MTT assay

Cell viability was evaluated using a range of concentrations of ZnO NPs (5–80 μg/ml) by MTT assay for two time periods; 6 and 24 h. Astrocytes exposed to ZnO NPs showed time and dose dependent reduction in mitochondrial activity (Fig. 3a). Astrocytes exposed with 20 and 100 μg/ml ZnO NPs exhibited a mitochondrial activity of 96.26 ± 5.45% and 54.45 ± 2.28 respectively at 6 h of exposure. This was further reduced to 70.90 ± 1.78 (20 μg/ml) and 27.83 ± 0.59% (100 μg/ml) at 24 h. The lethal concentration (LC50) was found to be 60 μg/ml (49.26 ± 1.85).

3.6.2. NRU assay

Comparable to that of MTT assay, NRU assay results showed a dose dependent decrease in lysosomal activity at 6 h and 24 h of exposure. The drop in lysosomal activity was more pronounced at 24 h of incubation (Fig. 3b). Upon exposure of 30 μg/ml of ZnO NPs for 6 h, percentage of lysosomal activity was 86.01 ± 1.98 which gradually reduced to 61.51 ± 2.77 at 24 h of exposure. The percentage cell viability was below 50% in 100 μg/ml ZnO NPs treated cells at 6 h

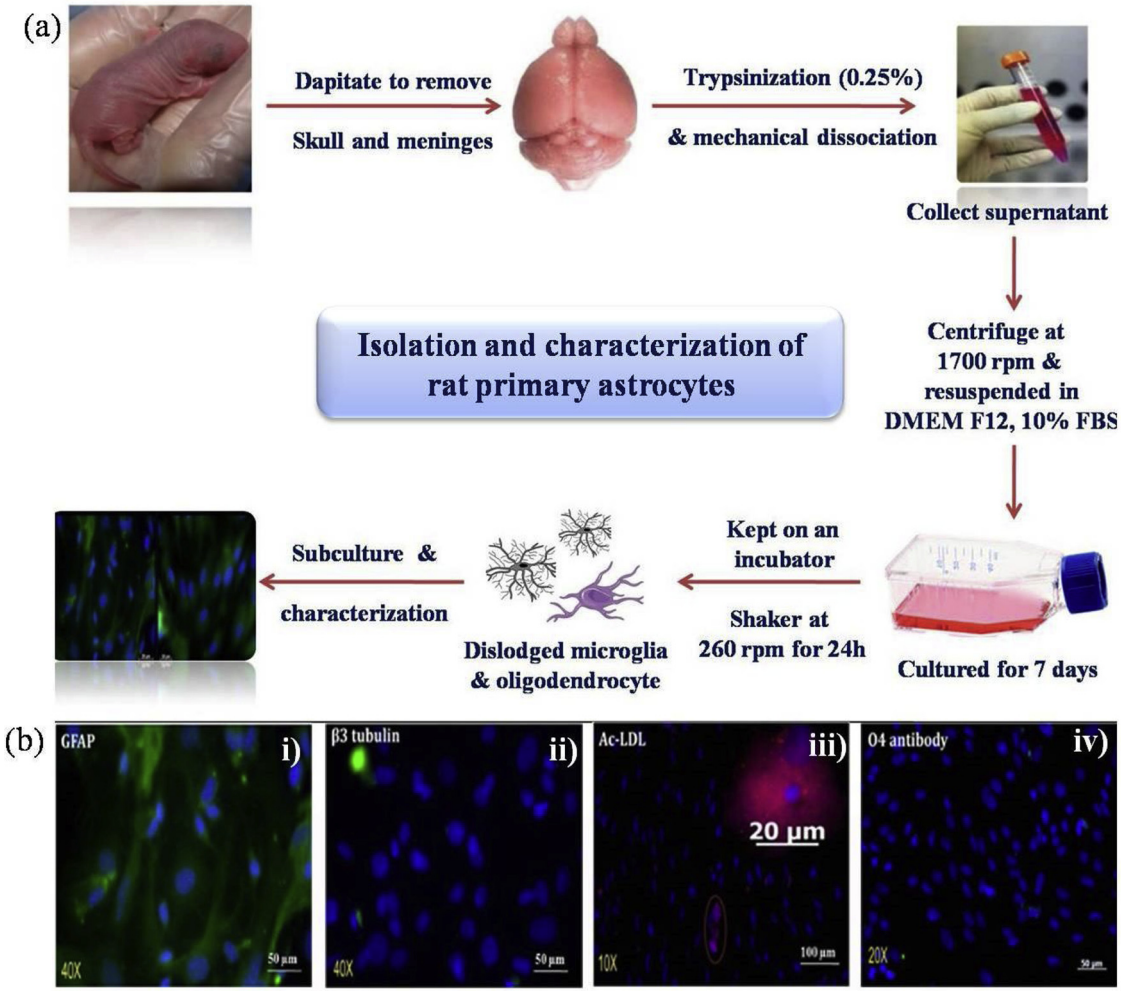

Fig. 2. (a) Isolation and purification of astrocytes from post-natal 0–2 day old rat pup (b) Characterisation of primary astrocytes isolated from 0 to 2 day old rat pups. Astrocyte specific marker GFAP (i), neuronal marker β3 tubulin (ii), Ac-LDL (iii) and oligodendrocyte marker O4 antibody (iv) metabolised by microglia and endothelial cells are used. The cells in red circle are positive for Ac-LDL. Scale bar and Magnification: 50 μm and 40X (for Fig. 2b (i)), 100 μm and 10X for Fig. 2b (iii), 50 μm and 20X for Fig. 2b (iv).

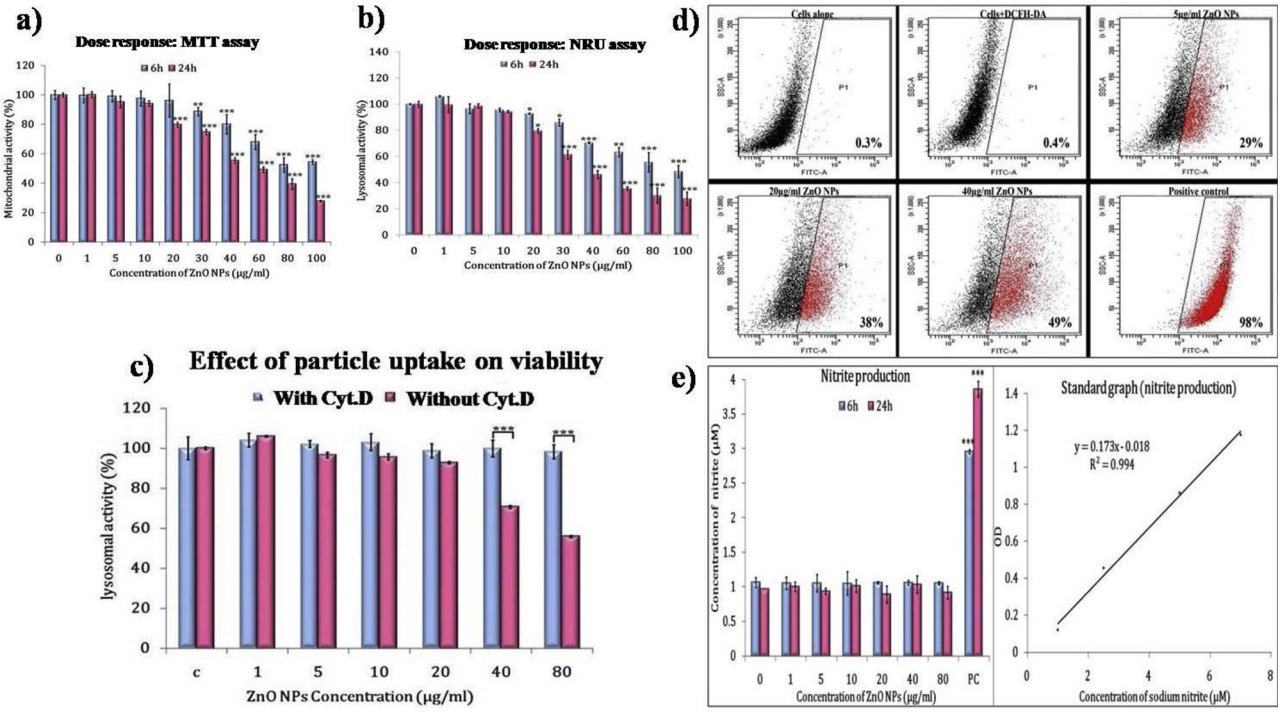

Fig. 3. (a) Dose response of primary astrocytes exposed to ZnO NPs for 6 h and 24 h by MTT assay (b) Dose response of primary astrocytes exposed to ZnO NPs for 6 h and 24 h by NRU assay (c) Particle uptake in presence of inhibitor cytochalasin D: effect of ZnO NPs uptake on mitochondrial activity of primary astrocytes. Cells were exposed to ZnO NPs for 6 h. 4µM cytochalasin D pre-treatment for 1 h was used as inhibitor of endocytosis (d) Formation of reactive oxygen species in primary astrocytes exposed to ZnO NPs for 6 h. P1 quadrant represents population that is positive for DCFH-DA. H_2O_2 treated cells were used as positive control. n = 3 (e) RNS production by Griess reagent assay showing nitrite production in primary astrocytes exposed to ZnO NPs for 6 and 24 h. LPS treated samples were used as positive control. The data represent mean ± SD of three independent experiments. Asterisk denotes statistically significant difference (***$p < 0.001$).

(48.59 ± 3.69) and 24 h (27.79 ± 5.14). The LC50 determined from NRU assay was 40 µg/ml.3

3.7. Particle uptake in presence of inhibitor

Particle uptake was confirmed using the endocytosis inhibitor Cyt.D. ZnO NP mediated cytotoxicity was considerably amelioratred by Cyt.D. A statistically significant difference in viability was observed for 40 and 80 µg/ml ZnO NPs treated cells in presence of cytochalasin D (Fig. 3c). It was observed that the viability of 80 µg/ml treated cells was dropped to 55.82 ± 0.52, whereas cytochalasin D pre-treated group showed 98.34 ± 3.04 viability.

3.8. Cell morphology analysis by Giemsa staining

Time and dose responsive alterations in astrocyte's morphology was analysed by Giemsa staining (Fig. 4a). Shrinkage of cytoplasm was seen in 80 µg/ml treated cells at 6 h, without any structural changes in nuclear compartment. Cell density was severely affected in 40 and 80 µg/ml treated cells at 24 h. Complete disintegration of cytoplasm morphology along with nuclear condensation was observed in both 40 and 80 µg/ml treated cells. Cells retained its morphology comparable to that of control cells when treated with 20 µg/ml for both 6 and 24 h of incubation.

3.9. Cytoskeletal analysis by rhodamine phalloidin staining

Rhodamine phalloidin staining evidenltly proved significant levels of cytoskeletal changes in astrocytes upon NP exposure (Fig. 4b). Deterioration of stress fibres along with changes in focal adhesions were observed for 80 µg/ml treatment group at 6 h of incubation. All other treated cells exhibited cytoskeletal morphology similar to that of control at 6 h. 40 µg/ml (24 h) treatment displayed severe alterations in cytoskeletal structure with disappearance of stress fibres and modifications in focal adhesion points. Cell density was markedly low in 80 µg/ml treatment group with complete loss of focal adhesion centres and stress fibres.

3.10. Detection of reactive oxygen species (ROS) by DCFH-DA

ROS generation in presence of ZnO NPs was estimated using the probe DCFH-DA and it confirmed a dose dependent increase in ROS (Fig. 3d). The lowest concentration of ZnO NPs (5µ/ml) exhibited 29% increase in ROS production whereas the 20 and 40 µg/ml showed 38% and 49% respectively. Negative and positive control cells exhibited 0.4 and 98% increase in ROS respectively.

3.11. Detection of reactive nitrogen species (RNS) by Griess reagent assay

RNS production in presence of ZnO NPs was analysed using Griess reagent assay. The positive control (LPS) treated cells exhibited a statistically significant increase in RNS production with respect to control. However, ZnO NPs did not induce RNS production in astrocytes. The values were similar in both control and treated cells (Fig. 3e).

3.12. Lysosomal integrity by acridine orange

Influence of ZnO NP exposure in lysosomal integrity of astrocytes was analysed by AO staining. Exposure of ZnO NPs for duration of 6 h caused a dose dependent lysosomal destabilisation in astrocytes (Fig. 5a). Reduction in red fluorescence of AO indicted severe loss of lysosomes when exposed to 80 µg/ml of ZnO NPs.

3.13. Mitochondrial membrane potential by JC1 staining

MMP of particle exposed astrocytes was microscopically analysed

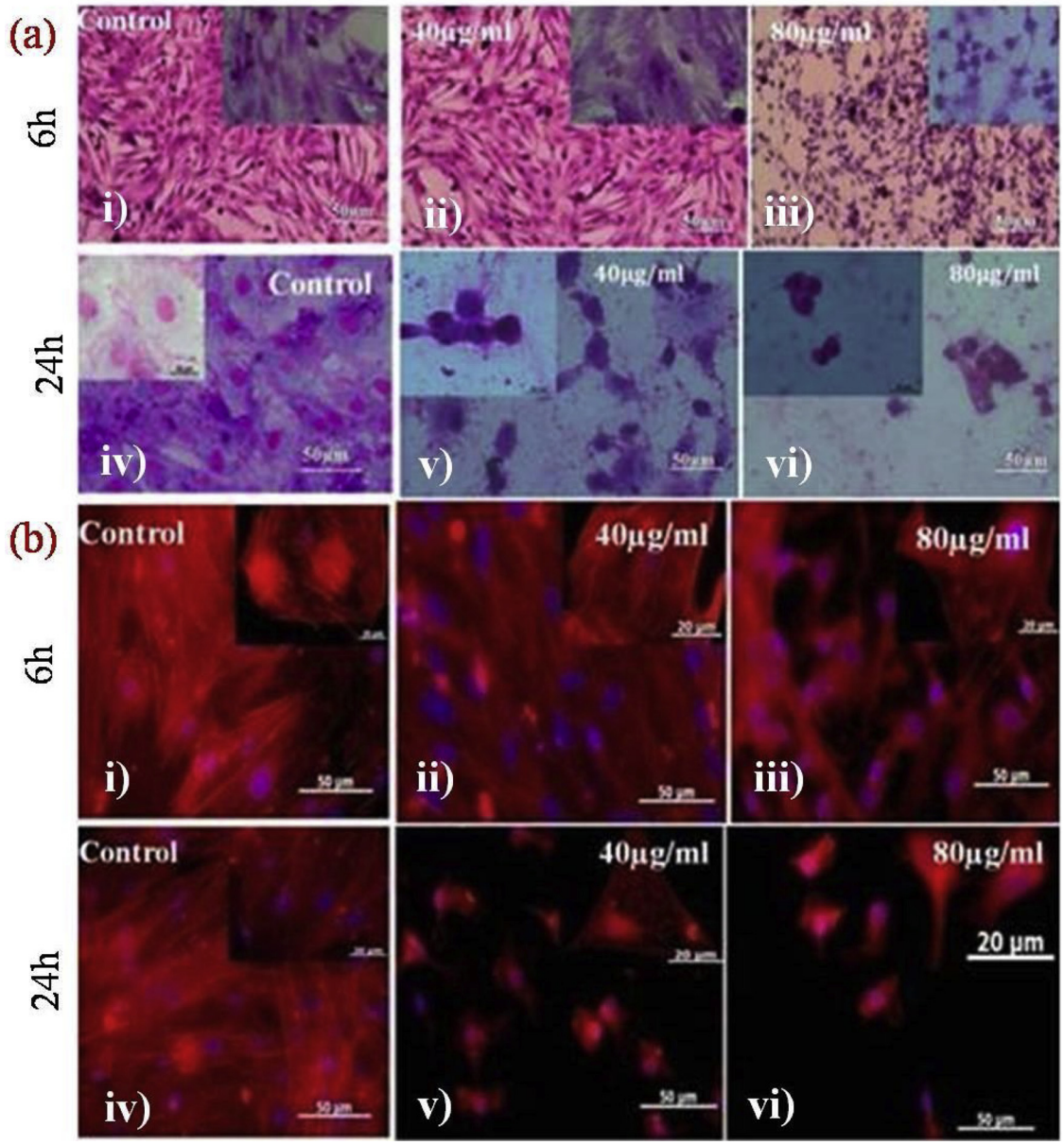

Fig. 4. Morphology of primary astrocytes exposed to ZnO NPs by staining with (a) Giemsa; Row one (6 h): i) Control ii) 40 µg/ml iii) 80 µg/ml, Row two (24 h): iv) Control v) 40 µg/ml vi) 80 µg/ml. (b) Rhodamine phalloidin; Row one (6 h): i) Control ii) 40 µg/ml iii) 80 µg/ml, Row two (24 h): iv) Control v) 40 µg/ml vi) 80 µg/ml. Figure in the inset shows high magnification images of respective treatment group. 6 h micrograph; scale bar: 100 µm, magnification 20 × . 6 h inset; scale bar 50 µm and magnification 40 × . 24 h micrograph: scale bar 50 µm and magnification 40 × . 24 h inset scale bar represents 20 µm and magnification 63 × .

by JC1 staining using red and green filters. NP induced decline in MMP in a dose and time dependent manner was observed in astrocytes (Fig. 5b). Very few number of cells belonging to 40 and 80 µg/ml treatment group exhibited marked reduction MMP at 24 h. Clumped mitochondria were evident in all treated cells at 6 and 24 h; whereas active and healthy mitochondria in diffused appearance were observed in the control groups.

3.14. Apoptosis by annexin V/PI staining

Annexin V/PI staining was used to evaluate apoptosis in astrocytes. Appropriate controls were used to gate the population. There was a dose dependent increase in annexin V positive cells and annexin V/PI double positive cells (Fig. 6a). Statistically significant difference was observed in 20, 40 and 80 µg/ml treated cells with respect to control (cells alone).

3.15. Caspase 3/7 activation assay

NP induced cellular apoptosis was analysed by mapping the caspase 3/7 pathway. Caspase 3/7 activity in response to ZnO NPs was measured fluorometrically. There occured a dose dependent increase in caspase 3/7 activity when exposed to ZnO NPs in astrocytes. 80 µg/ml of ZnO NPs induced a statistically significant increase in caspase activity (71.94 ± 3.83%) compared to control (Fig. 6b).

3.16. Cell membrane integrity by calcein AM-PI staining

The event of membrane permeabilisation and cell viability was analysed using Calcein AM -PI staining. 80 µg/ml of ZnO NPs exposure for 6 h elicited membrane permeabilisation in astrocytes. However, the cells remained positive for Calcein at 80 µg/ml concentration. Membrane integrity remained intact for all other concentration (up to 40 µg/ml) at 6 h of exposure. There was only negligible number of PI

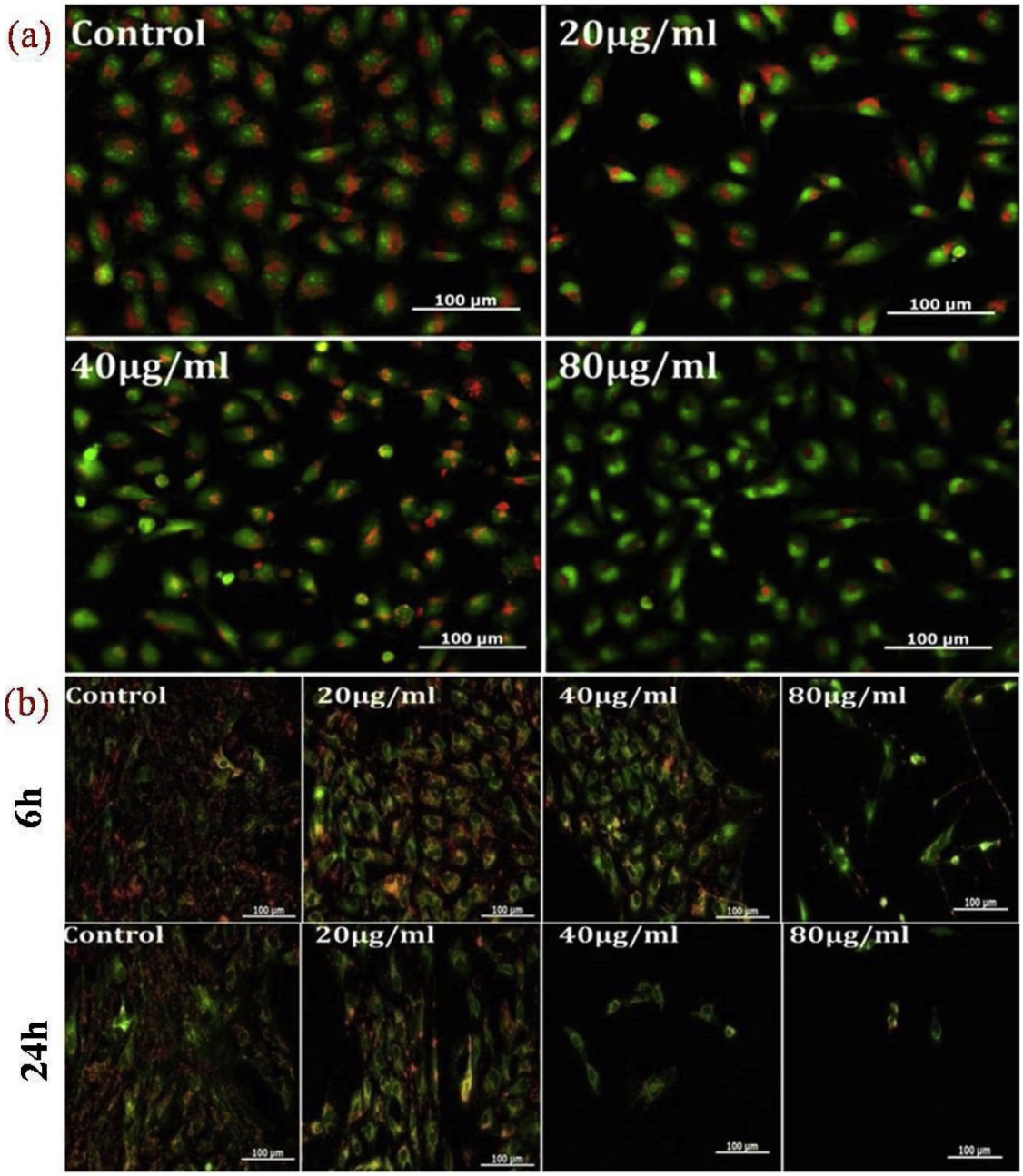

Fig. 5. (a) Lysosomal integrity in primary astrocytes exposed to ZnO NPs for 6 h. Untreated cells were used as control. The green signal indicates the cytoplasm. Red signal shows the lysosomes (b) MMP analysis of primary astrocytes cells exposed to ZnO NPs: Row one indicates 6 h and row two indicates 24 h respectively. Magnification 20X. (For interpretation of the references to colour in this figure legend, the reader is referred to the web version of this article.)

positive cells at 6 h period. ZnO NPs exposure (40 and 80 µg/ml) at 24 h exhibited rigorous loss of cell number and membrane integrity. Treated cells showed a positive response to PI whereas negative response to that of calcein; which further substantiate complete loss of cellular activity. Calcein positive cells with intact membrane were observed at 20 µg/ml treated cells (Fig. 6c).

3.17. Nuclear condensation by DAPI staining

Chromatin condensation in astrocytes was evaluated by DAPI staining after NP exposure. Cells showed nuclear condensation in a dose and time dependent manner (Fig. 6d). Significant nuclear condensation was observed for those cells treated with 40 and 80 µg/ml of ZnO NP after 24 h; whereas no such findings were originated in rest of the treatment groups. Meanwhile, 6 h of incubation was enough for ZnO NPs to induce chromatin condensation at 80 µg/ml concentartion.

3.18. Effect of particle size and dissolution on astrocytes

3.18.1. Cytotoxicity by MTTassay

Effect of particle dissolution and size on the biological interaction of ZnO NPs was evaluated by comparing the mitochondrial activity among ZnO NPs, zinc ion ($ZnCl_2$) and bulk form of ZnO. The bulk formulation exhibited least toxicity when compared $ZnCl_2$ and ZnO NPs. On the other hand $ZnCl_2$ treated cells showed a similar pattern of mitochondrial activity at 6 h (Fig. 7a) and 24 h (Fig. 7b).

3.18.2. Cell count by trypan blue exclusion assay

Cell count was determined by trypan blue exclusion assay. The cell count in the culture after ZnO NPs exposure was compared with culture

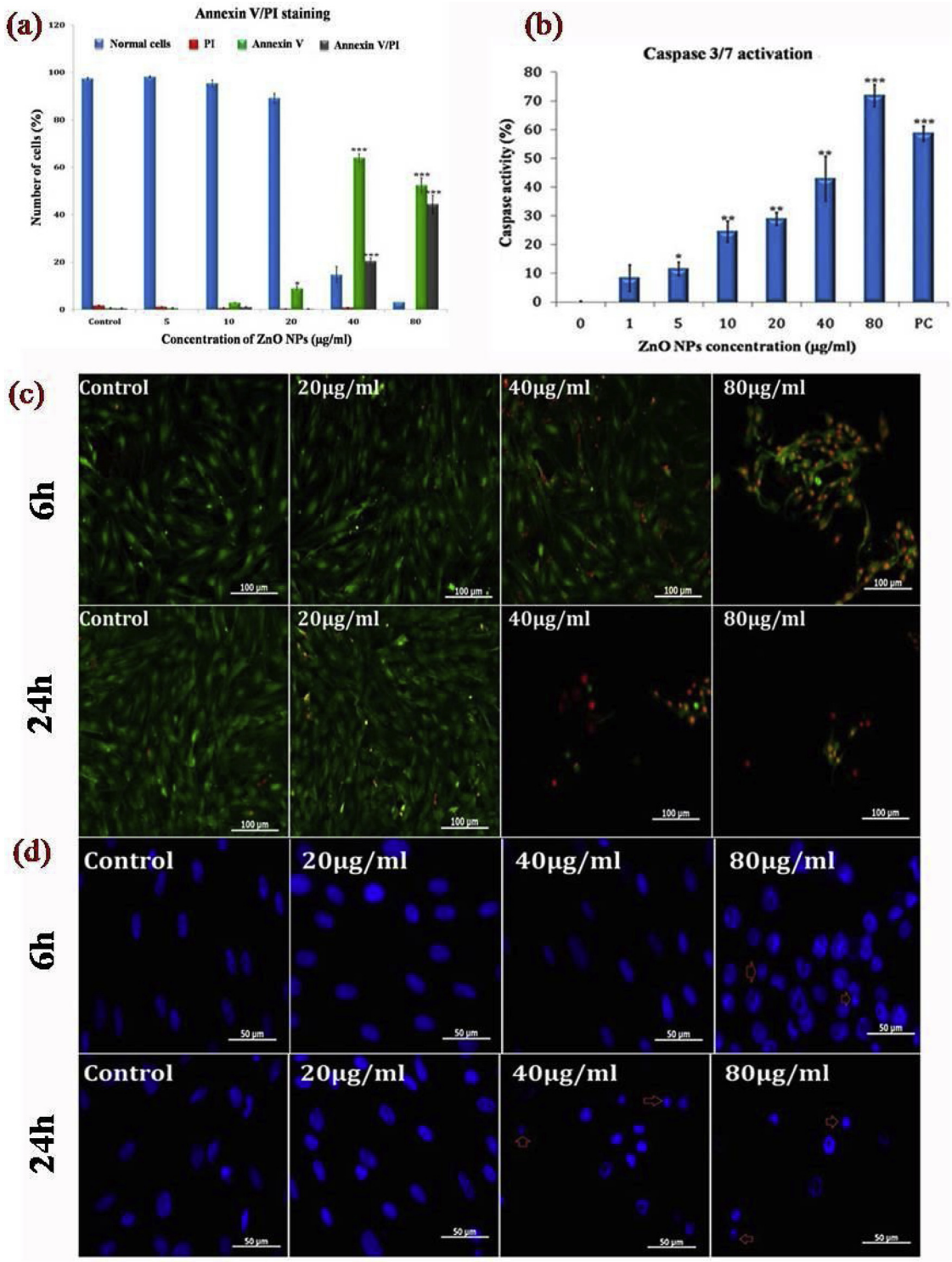

Fig. 6. (a) Apoptosis by annexin V/PI staining of astrocytes exposed to ZnO NPs (b) Caspase mediated apoptosis by caspase 3/7 activity in astrocytes exposed to ZnO NPs. The data represent mean ± SD of three independent experiments. Asterisk above columns denotes statistically significant difference, compared to the control group (*$p < 0.001$, **$p < 0.001$ and ***$p < 0.001$) (c) Cell membrane integrity of astrocytes treated with ZnO NPs for 6 h and 4 h by Calcein AM/PI staining of cells. Green signal indicate viable and red signal indicate membrane disintegrated cells (d) Nuclear condensation by DAPI staining in primary astrocytes exposed to ZnO NPs for 6 h and 24 h. Untreated astrocytes used as control. Scale bar represents 100 µm. Magnification 20×. (For interpretation of the references to colour in this figure legend, the reader is referred to the web version of this article.)

exposed to $ZnCl_2$ and bulk formulation of ZnO. The nano formulation of ZnO showed significant reduction in the total cell count at 40 and 80 µg/ml. It was also noticeable that the total cell count was varied significantly in $ZnCl_2$, bulk and nanoformulation. More number of dead cells was visible in ZnO bulk treated cells when compared to ZnO NPs and $ZnCl_2$ treated cells. Cell count was more or less similar in $ZnCl_2$ and ZnO NPs treated cells except at 80 µg/ml (Fig. 7c).

3.18.3. *Detection of ROS by DCFH-DA assay*

Astrocytes exposed to ZnO NPs, $ZnCl_2$ and ZnO bulk particles were

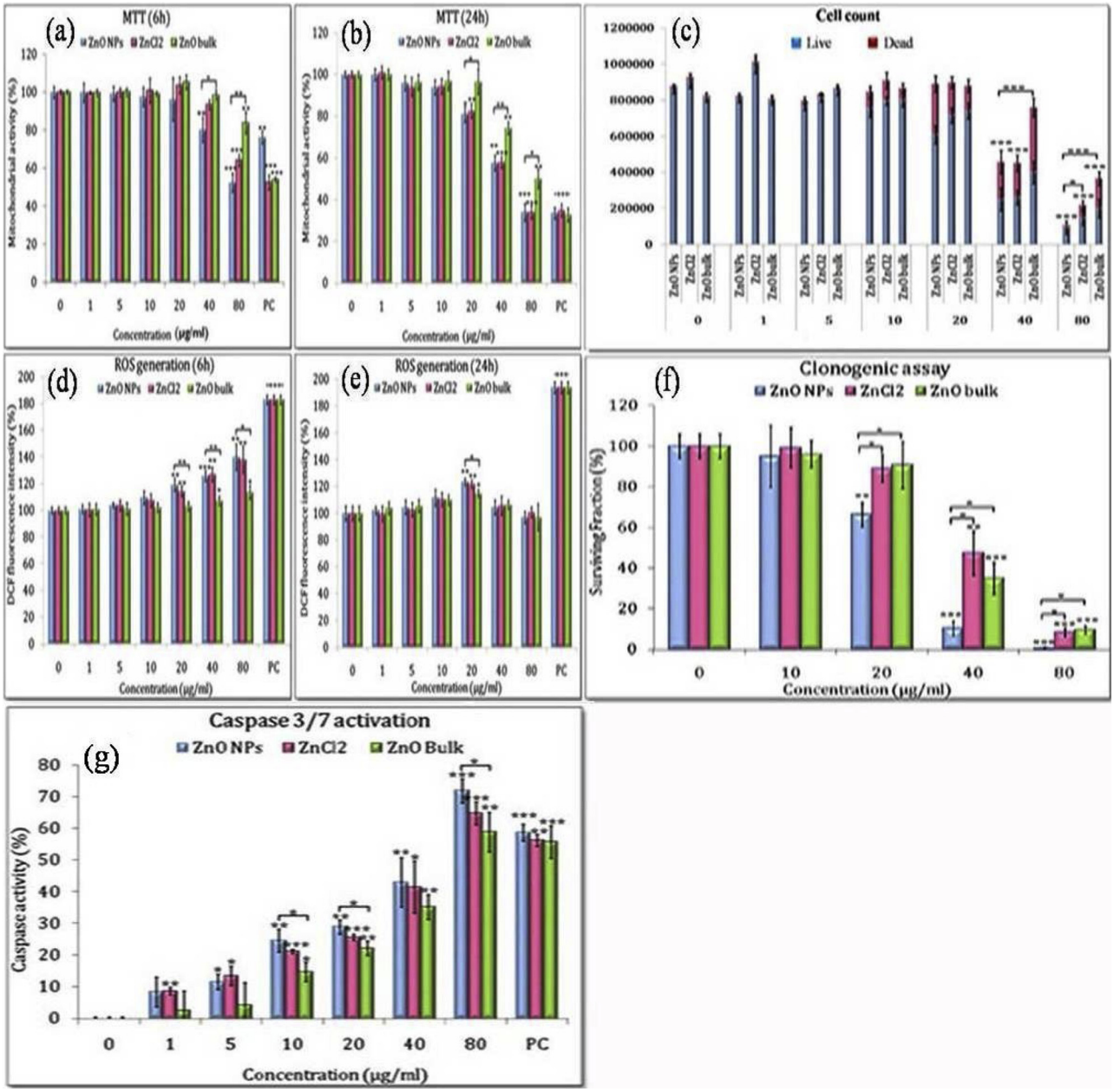

Fig. 7. Mitochondrial activity of primary astrocytes exposed to ZnO NPs, $ZnCl_2$ and ZnO bulk particle for (a) 6 h and (b) 24 h. Phenol treated cells were used as positive control. The values are expressed in percentage with respect to control (c) Trypanblue exclusion assay comparing the cell count in primary astrocytes exposed to ZnO NPs, $ZnCl_2$ and ZnO bulk for 24 h. Comparison of ROS generation in primary astrocytes exposed to ZnO NPs, $ZnCl_2$ and ZnO bulk for (d) 6 h and (e) 24 h analysed by DCFH-DA. H_2O_2 treated cells were used as positive control. (f) Comparison of regenerative and proliferation potential of primary astrocytes exposed to ZnO NPs, $ZnCl_2$ and ZnO bulk using clonogenic assay (g) Comparison of caspase 3/7 activation in primary astrocytes exposed to ZnO NPs, $ZnCl_2$ and ZnO bulk formulation for 24 h. The values are expressed in percentage fluorescence with respect to control. The data represent mean ± SD of three independent experiments. Asterisk denotes statistically significant difference (*$p < 0.05$, **$p < 0.01$ and ***$p < 0.001$).

compared in terms of ROS generation. At 6 h of exposure, ZnO NPs caused the cells to generate higher amount of ROS than ZnO bulk particles (Fig. 7d). The $ZnCl_2$ exposed groups responded similar to that of ZnO NPs. At 24 h of incubation, all the three types of particles induced a slender reduction in ROS levels (Fig. 7e), which could be attributed to the elevated levels of cytotoxicity for longer peroid of exposure.

3.18.4. Evaluation of proliferative capacity and survival rate by Clonogenic assay

Clonogenic assay was performed to detect the cell survival and proliferation potential of the cells. The results of the Clonogenic assay of ZnO NPs were compared with $ZnCl_2$ and ZnO bulk exposed cells. Cells exposed to higher concentration of ZnO NPs exhibited low survival rate and proliferation potential compared to $ZnCl_2$ and ZnO bulk form. This is due to the low number of colonies formed in ZnO NPs treated cells (Fig. 7f).

3.18.5. Evaluation of apoptosis by Caspase 3/7 activation assay

Caspase 3/7 activation assay was performed to analyse the degree of induced caspase activity in astrocytes. Astrocytes exhibited a dose dependent increase in caspase activity when exposued with ZnO NPs, $ZnCl_2$ and ZnO bulk formulation (Fig. 7g). However, the effect was directly linked to the total cells. It was observed that ZnO NPs induced a

significantly high caspase activity when compared to $ZnCl_2$ and ZnO bulk formulation.

4. Discussion

ZnO NPs has by now grown to be one of the commercially important and widely employed NPs with spectrum of applications in areas like daily care products, sensors, ceramics and rubber industries, food packages, as anti-bacterial agent and in several biomedical sectors. Photocatalytic property of ZnO NPs makes them ideal candidate for cancer therapies (Zhang et al., 2013). One of the attractive features of ZnO NPs is that they can be synthesized easily in a variety of forms. ZnO NPs displaying different morphologies have been synthesized effectively using wet precipitation method by changing the parameters of the experiment including temperature, solute concentration, method of addition of reagents and pH (Kumar et al., 2013). For the present study, wet precipitation of zinc nitrate and zinc sulphate using NaOH yielded ZnO NPs possessing characteristic sphere head morphology (ZnO SP). Since physico-chemical properties of NPs would greatly influence its fate in biological system, synthesized ZnO NPs were characterised for its size, morphology, hydrodynamic diameter, surface area, charge, chemical composition and purity (Sánchez-Iglesias et al., 2006). As observed from SEM analysis, no aggregation was observed for ZnO SP. TEM analysis gave core size of the nanoparticle, and indicated narrow size distribution. DLS data indicated that size of ZnO SP remained intact for all concentrations tested and PDI was near to 0.1, suggesting moderately homogenous suspension (Gaumet et al., 2008). XPS analysis further confirmed purity of the synthesized NPs. Higher surface reactivity of NPs endows adsorption of biomolecules preferably. Hence biological characterization was executed which includes the detection of endotoxins (Smulders et al., 2012; Nel et al., 2009). It was found that endotoxin level in ZnO NPs was below 0.5EU/ml which is well below the USP mandated limits for biomaterials.

Tramping application possibilities of ZnO NPs inturn necessitates a comprehensive toxicity evaluation using different tissue/cell models. Bridging with this perception, a detailed *in vitro* study was designed for investigation of neurotoxic potential of ZnO NPs. Being an excellent cell model mimicking the exact phenotypes of neuronal cells *in vivo*, primary astrocytes isolated from post-natal 0–2 day old rat pups were used throughout the study. These are the major glial cells which maintain homeostasis in the brain. The cells were isolated from rat pups using the method described by Weinstein DE with slight modifications (Weinstein, 2001). The isolated primary astrocytes were maintained in the laboratory conditions and used for bio-interaction studies. Endothelial cells, microglia and neurons often accompany primary astrocyte culture which may contribute to erroneous results. Hence purity of the astrocytes used for the study was confirmed by immunostaining using markers like GFAP, B3 tubulin and O4 antibody.

The viability and dose response in astrocytes were investigated by MTT, NRU assays and further verified by trypan blue exclusion method. Treatment with a toxic component interferes with cell viability results in three different ways. The first one is the cytostatic effect of compound may inhibit the proliferative capacity of the cells. The second is an anti-adhesive effect where the cells detach from its substratum to adrift in the medium. Third mechanism is cytotoxicity where the compound interacts directly and kills the cells. Consistent with prevoius results (Bondarenko et al., 2013), both MTT and NRU assays revealed a time and dose dependent toxicity in cells suggesting reduced metabolic activity of the cells. The LC_{50} value obtained for the present study was 40 μg/ml, suggesting the higher sensitivity of primary astrocytes with ZnO NPs (Ivask et al., 2015).

Being a simple and reliable method reflecting the underlying toxicity mechanism exhibited by NPs, cellular morphology of exposed cells were analysed by Giemsa staining. Marked retraction of cytoplasm, nuclear condensation, cell shrinkage and reduction in cell density in a dose and time dependent manner were observed in particle treated astrocytes. Direct death/ deterioration of cells and decreased cell adhesion in the substratum are the two possible reasons for reduction in cell density. Rhodamine phalloidin staining was carried out to analyse the impact of NPs in cell adhesion propeties of astrocytes. An early dissociation of actin stress fibres and cytoskeletal rearrangement were specifically observed. Deterioration of stress fibres and loss of focal adhesion points observed in the study clearly indicated that the ZnO NPs adversely affect the adhesive properties of the cells (Seil and Webster, 2008). Flow cytometric analysis using pre-tretatment of astrocytes with the non-specific endocytosis marker Cyt. D revealed obvious reduction in cellular uptake of ZnO NPs which is in concordance with the previous results (Roy et al., 2014). Promising endocytic pathway further demands the need for the investigation of lysosomal membrane integrity in terms of lysosomal membrane permeabilization (LMP). AO staining revealed dose dependent reduction in LMP in astrocytes. Cho et al., in 2011 have reported similar incidence of ZnO NP mediated lysosomal destabilization and lung injury (Cho et al., 2011).

Free radical generation in astrocytes exposed to ZnO NPs was analysed using flow cytometry and results indicated that there occurred a dose dependent increase in DCF fluorescence. Certain molecules have been known for their capacity to induce astrocytes activation by nitric oxide production (Colombo et al., 2014). Zinc mediated nitric oxide production and inflammation has been linked to brain pathologies (McCord and Aizenman, 2014). In contrast, there was no detectable RNS generation in ZnO NP exposed astrocytes in present study. JC 1 staining revealed that ZnO NPs (40 and 80 μg/ml) induced a significant loss of MMP in astrocytes *via* concentration dependent manner. In addition, mitochondria was found to be clumped and scattered along the cytoplasmic extentions which indicates active rearrangement of actin filaments and hence supporting the data obtained for rhodamine phalloidin staining. It has previously been reported that the event of caspase activation and hence apoptosis is closely associated with loss of MMP (Lakhani et al., 2006). Caspase analysis for the present study indicated a dose and time dependent increase in caspase activity with the execution of apoptotic features like cytoplasmic shrinkage, retraction of pseudopodia, reduction of cellular volume (pyknosis) and membrane blebbing. The present findings are in agreement with previous reports of Kromer et al. (Kroemer et al., 2009). Further, the cells with disintegrated membrane did not indicate other necrotic features like cell swelling and cytoplasmic spillage. This finding rules out the co-existence of apoptosis and necrosis. Yuste et al. (Yuste et al., 2001) have proposed that DNA fragmentation can not always be a fitting symptom for cellular apoptosis. This fact was reproduced in the present study in which no substantial DNA fragmentation was observed. It is also likely that ZnO NPs directly degrade biological molecules, thereby making the detection of DNA ladder impossible.

A comparative study was carried out with ZnO NPs, $ZnCl_2$ and ZnO bulk particles to understand the influence particle size and dissolution on cytotoxicity. $ZnCl_2$ undergoes complete dissolution in physiological pH (~7) to release zinc ions (Zn^{2+}) thus this zinc salt was used to represent ionic counterpart of ZnO. Cell viability, cell number, ROS production and cell regeneration potential were compared among $ZnCl_2$, ZnO NPs and ZnO bulk treated astrocytes. Mitochondrial activity showed a significant difference among the ZnO NPs and ZnO bulk whereas $ZnCl_2$ behaved more or less similar to that of untreated control. ZnO bulk particle treated cells retained more cells compared to ZnO NPs and $ZnCl_2$. At high concentrations (40 and 80 μg/ml) the total number of cells (live and dead) were very low in $ZnCl_2$ and ZnO NPs treated samples. This finding ensures the higher reactivity of ZnO NPs with cellular components (Kim et al., 2010). In this context, both ROS generation and caspase activity were more pronounced during astrocyte exposure with ZnO NPs and $ZnCl_2$ than ZnO bulk form. Strikingly there formed more number of colonies in clonogenic assay for ZnO NPs more than ZnO bulk and $ZnCl_2$. This fact could be considered as one of the highlights of the study which endorses the nanospecific toxicity of ZnO NPs independent of its dissolution. This further point toward that ZnO

NPs exposure even for a short period can elicit serious adverse consequences in neuronal tissue.

5. Conclusion

Inorder to address the neurotoxic potential of ZnO NPs, an inclusive study was designed using primary astrocytes isolated from post-natal 0–2 day old rat pups which represent an ideal *in vivo* neuronal tissue. Wet precipitation method was adopted for the sysnthesis of ZnO NPs and characterized for size, shape, specific surface area, surface charge, hydrodynamic diameter, chemical structure and purity. According to the physico-chemical characterization data, the NPs were homogenously distributed and showed excellent colloidal stability in culture media tested. Biological characterization was also performed which ensured that the NPs were devoid of any endotoxins. The cells isolated from rat pups using the method described by Weinstein DE with slight modifications were used for bio-nano interaction studies. Purity of the astrocytes was then confirmed by immunostaining using markers like GFAP, B3 tubulin and O4 antibody. Cell viability assays (MTT, NRU and Trypan Blue exclusion assays) confirmed dose and time dependent reduction in cell viability upon ZnO NP exposure on astrocytes suggesting the metabolic instability. In connection with this observation, non-fluorescent and fluorescent staining methodologies were adopted (Giemsa and Rhodamine phalloidin staining respectively) inorder to evaluate the possible morphological alterations within the NP treated cells. Both confirmed marked reduction in cytoplasm, nuclear condensation, cell shrinkage as well as actin re-organization in a timely and dose dependent manner. Endocytic route of the NPs was confirmed using a non-specific endocytic marker Cyt.D and subsequent investigation on lysosomal alterations using AO staining ensured active LMP. Regarding NP induced free radical generation; momentous ROS production was confirmed by DCF probe while astrocytes remained negative for RNS evolution. MMP was found to be severely affected and induced the cell to undergo apoptosis. Interrupted ATP production and ensuing activation of caspase pathway turned the cells susceptible to apoptosis. Strikingly no active DNA fragmentation was evident which made certain that the NPs are not causing any damages within the nuclear premises. Comparitive study was conducted regarding the toxic potential of ZnO NPs, $ZnCl_2$ and ZnO bulk form. This also confirmed that ZnO NPs are capable of eliciting a nano specific toxicity irrespective of its dissolution. As a whole the present study effectively portrayed the detrimental consequences of ZnO NPs within the neuronal tissue and hence questions the safety facet of different application fields comprising ZnO NPs.

Conflicts of interest

The authors declare no conflict of interest.

Acknowledgements

The authors wish to express their thanks to the Director and Head, Biomedical Technology Wing, Sree Chitra Tirunal Institute for Medical Sciences and Technology, Trivandrum, Kerala, India for their support and for providing the infrastructure to carry out this work. Sruthi S and Athira SS thank University Grants Commission, CSIR- New Delhi for JRF financial support.

References

Bahuguna, Ashutosh, Khan, Imran, Bajpai, Vivek K., Kang, Sun Chul, 2017. MTT assay to evaluate the cytotoxic potential of a drug. Bangladesh J. Pharmacol. 12, 115–118.
Bao, G., Mitragotri, S., Tong, S., 2013. Multifunctional nanoparticles for drug delivery and molecular imaging. Annu. Rev. Biomed. Eng. 15, 253–282.
Biosciences, B.D., 2011. Detection of Apoptosis Using the BD Annexin V FITC Assay on the BD FACSVerse™ System, 23-13027-00.
Blackburn, D., Sargsyan, S., Monk, P.N., Shaw, P.J., 2009. Astrocyte function and role in motor neuron disease: a future therapeutic target? Glia 57, 1251–1264.
Bondarenko, O., Juganson, K., Ivask, A., Kasemets, K., Mortimer, M., Kahru, A., 2013. Toxicity of Ag, CuO and ZnO nanoparticles to selected environmentally relevant test organisms and mammalian cells in vitro: a critical review. Arch. Toxicol. 87, 1181–1200.
Borenfreund, E., Puerner, J.A., 1985. Toxicity determined in vitro by morphological alterations and neutral red absorption. Toxicol. Lett. 24, 119–124.
Bryan, N.S., Grisham, M.B., 2007. Methods to detect nitric oxide and its metabolites in biological samples. Free Radic. Biol. Med. 43 (5), 645–657.
Buzea, C., Pacheco, I.I., Robbie, K., 2007. Nanomaterials and nanoparticles: sources and toxicity. Biointerphases 2, MR17–MR71.
Chang, Y.-N., Zhang, M., Xia, L., Zhang, J., Xing, G., 2012. The toxic effects and mechanisms of CuO and ZnO nanoparticles. Materials 5, 2850–2871.
Cho, W.-S., Duffin, R., Howie, S.E., Scotton, C.J., Wallace, W.A., MacNee, W., Bradley, M., Megson, I.L., Donaldson, K., 2011. Progressive severe lung injury by zinc oxide nanoparticles; the role of Zn 2+ dissolution inside lysosomes. Part. Fibre Toxicol. 8, 1.
Colombo, E., Di Dario, M., Capitolo, E., Chaabane, L., Newcombe, J., Martino, G., Farina, C., 2014. Fingolimod may support neuroprotection via blockade of astrocyte nitric oxide. Ann. Neurol. 76, 325–337.
De Simone, U., Manzo, L., Profumo, A., Coccini, T., 2013. In vitro toxicity evaluation of engineered cadmium-coated silica nanoparticles on human pulmonary cells. J. Toxicol. 2013.
Deng, X., Luan, Q., Chen, W., Wang, Y., Wu, M., Zhang, H., Jiao, Z., 2009. Nanosized zinc oxide particles induce neural stem cell apoptosis. Nanotechnology 20, 115101.
Foo, L.C., Allen, N.J., Bushong, E.A., Ventura, P.B., Chung, W.-S., Zhou, L., Cahoy, J.D., Daneman, R., Zong, H., Ellisman, M.H., 2011. Development of a method for the purification and culture of rodent astrocytes. Neuron 71, 799–811.
Fröhlich, Eleonore, 2018. Comparison of conventional and advanced in vitro models in the toxicity testing of nanoparticles. Artif. Cells Nanomed. Biotechnol. 1–17.
Gaumet, M., Vargas, A., Gurny, R., Delie, F., 2008. Nanoparticles for drug delivery: the need for precision in reporting particle size parameters. Eur. J. Pharm. Biopharm. 69, 1–9.
Hanley, C., Layne, J., Punnoose, A., Reddy, K., Coombs, I., Coombs, A., Feris, K., Wingett, D., 2008. Preferential killing of cancer cells and activated human T cells using ZnO nanoparticles. Nanotechnology 19, 295103.
Hernández-Sierra, J.F., Ruiz, F., Pena, D.C.C., Martínez-Gutiérrez, F., Martínez, A.E., Guillén, AdJP, Tapia-Pérez, H., Castañón, G.M., 2008. The antimicrobial sensitivity of Streptococcus mutans to nanoparticles of silver, zinc oxide, and gold. Nanomedicine 4, 237–240.
Ivask, A., Titma, T., Visnapuu, M., Vija, H., Kakinen, A., Sihtmae, M., Pokhrel, S., Madler, L., Heinlaan, M., Kisand, V., 2015. Toxicity of 11 metal oxide nanoparticles to three mammalian cell types in vitro. Curr. Top. Med. Chem. 15, 1914–1929.
Kim, I.-S., Baek, M., Choi, S.-J., 2010. Comparative cytotoxicity of Al2O3, CeO2, TiO2 and ZnO nanoparticles to human lung cells. J. Nanosci. Nanotechnol. 10, 3453–3458.
Kroemer, G., Galluzzi, L., Vandenabeele, P., Abrams, J., Alnemri, E., Baehrecke, E., Blagosklonny, M., El-Deiry, W., Golstein, P., Green, D., 2009. Classification of cell death: recommendations of the Nomenclature Committee on Cell Death 2009. Cell Death Differ. 16, 3–11.
Kumar, S.S., Venkateswarlu, P., Rao, V.R., Rao, G.N., 2013. Synthesis, characterization and optical properties of zinc oxide nanoparticles. Int. Nano Lett. 3, 30.
Lakhani, S.A., Masud, A., Kuida, K., Porter, G.A., Booth, C.J., Mehal, W.Z., Inayat, I., Flavell, R.A., 2006. Caspases 3 and 7: key mediators of mitochondrial events of apoptosis. Science 311, 847–851.
Manke, A., Wang, L., Rojanasakul, Y., 2013. Mechanisms of nanoparticle-induced oxidative stress and toxicity. Biomed Res. Int. 2013.
McCord, M.C., Aizenman, E., 2014. The role of intracellular zinc release in aging, oxidative stress, and Alzheimer's disease. Front. Aging Neuro. Sci. 6.
Narkiewicz, U., Sibera, D., Kuryliszyn-Kudelska, I., Kilanski, L., Dobrowolski, W., Romcevie, N., 2008. Synthesis by wet chemical method and characterization of nanocrystalline ZnO doped with Fe2O3. Acta Phys. Pol. 113 (6), 1695–1700.
Nel, A.E., Mädler, L., Velegol, D., Xia, T., Hoek, E.M., Somasundaran, P., Klaessig, F., Castranova, V., Thompson, M., 2009. Understanding biophysicochemical interactions at the nano–bio interface. Nat. Mater. 8, 543–557.
Nohynek, G., Dufour, E., Roberts, M., 2008. Nanotechnology, cosmetics and the skin: is there a health risk? Skin Pharmacol. Physiol. 21, 136–149.
Panyala, N.R., Peña-Méndez, E.M., Havel, J., 2009. Gold and nano-gold in medicine: overview, toxicology and perspectives. J. Appl. Biomed. 7, 75–91.
Perelman, A., Wachtel, C., Cohen, M., Haupt, S., Shapiro, H., Tzur, A., 2012. JC-1: alternative excitation wavelengths facilitate mitochondrial membrane potential cytometry. Cell Death Dis. 3, 1–7.
Reshma, S.C., Syama, S., Mohanan, P.V., 2016. Nano-biointeractions of PEGylated and bare reduced grapheneoxideon lung alveolar epithelial cells: a comparative in vitro study. Colloids Surf. B 140, 104–116.
Roy, R., Parashar, V., Chauhan, L., Shanker, R., Das, M., Tripathi, A., Dwivedi, P.D., 2014. Mechanism of uptake of ZnO nanoparticles and inflammatory responses in macrophages require PI3K mediated MAPKs signaling. Toxicol. In Vitro 28, 457–467.
Sánchez-Iglesias, Pastoriza-Santos, Pérez-Juste, Rodríguez-González, Garcia de Abajo, F.J., Liz-Marzán, L.M., 2006. Synthesis and optical properties of gold nanodecahedra with size control. Adv. Mater. 18 (19), 2529–2534.
Schummer, Joachim, 2004. Multidisciplinarity, interdisciplinarity, and patterns of research collaboration in nanoscience and nanotechnology. Scientometrics 59 (3), 425–465.
Seil, J.T., Webster, T.J., 2008. Decreased astroglial cell adhesion and proliferation on zinc oxide nanoparticle polyurethane composites. Int. J. Nanomedicine 3, 523–531.
Sirelkhatim, A., Mahmud, S., Seeni, A., Kaus, N.H.M., Ann, L.C., Bakhori, S.K.M., Hasan, H., Mohamad, D., 2015. Review on zinc oxide nanoparticles: antibacterial activity

and toxicity mechanism. Nano-Micro Lett. 7, 219–242.
Smulders, S., Kaiser, J.-P., Zuin, S., Van Landuyt, K.L., Golanski, L., Vanoirbeek, J., Wick, P., Hoet, P.H., 2012. Contamination of nanoparticles by endotoxin: evaluation of different test methods. Part. Fibre Toxicol. 9, 41.
Soenen, S.J., Rivera-Gil, P., Montenegro, J.-M., Parak, W.J., De Smedt, S.C., Braeckmans, K., 2011. Cellular toxicity of inorganic nanoparticles: common aspects and guidelines for improved nanotoxicity evaluation. Nano Today 6, 446–465.
Sohaebuddin, S.K., Thevenot, P.T., Baker, D., Eaton, J.W., Tang, L., 2010. Nanomaterial cytotoxicity is composition, size, and cell type dependent. Part. Fibre Toxicol. 7 (1), 22.
Toné, Shigenobu, Sugimoto, Kenji, Tanda, Kazue, Suda, Taiji, Uehira, Kenzo, Kanouchi, Hiroaki, Samejima, Kumiko, Minatogawa, Yohsuke, Earnshaw, William C., 2007. Three distinct stages of apoptotic nuclear condensation revealed by time-lapse imaging, biochemical and Electron microscopy analysis of cell-free apoptosis. Exp. Cell Res. 313 (16), 3635–3644.
Valdiglesias, V., Costa, C., Kiliç, G., Costa, S., Pásaro, E., Laffon, B., Teixeira, J.P., 2013. Neuronal cytotoxicity and genotoxicity induced by zinc oxide nanoparticles. Environ. Int. 55, 92–100.
Vance, M.E., Kuiken, T., Vejerano, E.P., McGinnis, S.P., Hochella Jr, M.F., Rejeski, D., Hull, M.S., 2015. Nanotechnology in the real world: redeveloping the nanomaterial consumer products inventory. Beilstein J. Nanotechnol. 6, 1769–1780.
Wan, C.P., Myung, E., Lau, B.H., 1993. An automated microfluorometric assay for monitoring oxidative burst activity of phagocytes. J. Immunol. Methods 159, 131–138.
Wang, Z.L., 2004. Zinc oxide nanostructures: growth, properties and applications. J. Phys. Condens. Matter 16, R829.
Weinstein, D.E., 2001. Isolation and purification of primary rodent astrocytes. Curr. Protoc. Neurosci. 3.5 1-3.5.9.
Xie, Y., Wang, Y., Zhang, T., Ren, G., Yang, Z., 2012. Effects of nanoparticle zinc oxide on spatial cognition and synaptic plasticity in mice with depressive-like behaviors. J. Biomed. Sci. 19, 1.
Yuste, Vc J., Bayascas, J.R., Llecha, N., Sánchez-López, I., Boix, J., Comella, J.X., 2001. The absence of oligonucleosomal DNA fragmentation during apoptosis of IMR-5 neuroblastoma cells DISAPPEARANCE OF THE CASPASE-ACTIVATED DNase. J. Biol. Chem. 276, 22323–22331.
Zhang, Y., Nayak, T.R., Hong, H., 2013. Biomedical applicationsof zinc oxide nanomaterials. Curr. Mol. Med 131633-45.